Available online at www.sciencedirect.com
SCIENCE DIRECT®
PERGAMON
International Journal of Heat and Mass Transfer 46 (2003) 3815–3830
International Journal of HEAT and MASS TRANSFER
www.elsevier.com/locate/ijhmt

Parametric study of unsteady flow and heat transfer in a pin-fin heat exchanger

A.K. Saha, Sumanta Acharya *

Department of Mechanical Engineering, Louisiana State University, Baton Rouge, LA 70803-6413, USA

Received 17 January 2003; received in revised form 28 March 2003

Abstract

A numerical study has been carried out to analyze the unsteady three-dimensional flow and heat transfer in a parallel-plate channel heat exchanger with in-line arrays of periodically mounted rectangular cylinders (pins) at various Reynolds number and geometrical configurations. The three-dimensional unsteady Navier–Stokes and energy equations are solved using higher order temporal and spatial discretizations. The simulations have been carried out for a range of Reynolds number based on cylinder width (180–600) and a Prandtl number of 6.99 (corresponding to water). Conjugate heat transfer calculations have been employed to account for the conduction in the solid cylinder and convection in the fluid. The thermal performance factor (TPF) increases significantly when the flow becomes unsteady. The choice of aspect ratio of the cylinders is judged by their relative increase in friction factor and heat transfer at transitional Reynolds number. The TPF is found to increase with the increase in pitch of the cylinders. The increase in channel height enhances the TPF though the heat transfer decreases at higher channel height.

1. Introduction

Efficient cooling of electronic components and turbine blades are important for their reliable performance. Compact heat exchangers, due to their high surface area per unit volume, and high heat transfer effectiveness, can provide some unique advantages in cooling strategies. Pin-fin heat exchangers or cooling passages, if fabricated at micro- or meso-scales, can be construed as compact heat exchangers, and combine the advantages of design simplicity and high effectiveness. The present paper reports the results of a three-dimensional numerical study in a heat exchanger passage with rectangular-cross-section pin fins. Both the steady and unsteady flow regimes in the periodically developed regions have been investigated for an in-line array of fins.

Compact heat exchangers are designed to provide high heat transfer surface area per unit volume and to alter the fluid dynamics to enhance mixing. Vortex generators such as fins, ribs or delta wings have been commonly used since they interrupt the thermal boundary layer, enhance turbulence levels and provide additional surface area for heat transfer. Heat transfer enhancement can also be achieved by promoting the large-scale unsteadiness or vortical structures due to primary and secondary instabilities in the flow. The generation and orientation of the vortices in the flow depends on the type of vortex generator or modification made to the heat exchangers. Spanwise vortices, typically two-dimensional in nature, orient themselves parallel to the axis of the vortex generators [1] (e.g., cylinders, aerofoils, etc.). On the other hand longitudinal vortices (oriented in the flow direction) give rise to three-dimensional flow even at a low Reynolds number [2]. An extensive review of the application of vortex generators for compact heat exchangers is given in Fiebig [3]. Experimental [4] and numerical simulation [5] of these oscillatory flows indicate that the heat transfer enhancement along the channel walls is due to the combined effects of the added surface area, the interruption of the wall boundary layers and the higher mixing

* Corresponding author. Tel.: +1-225-578-5809; fax: +1-225-578-5924.
E-mail address: acharya@me.lsu.edu (S. Acharya).

0017-9310/03/$ - see front matter © 2003 Elsevier Ltd. All rights reserved.
doi:10.1016/S0017-9310(03)00190-X

Nomenclature

A	breadth of the cylinder
B	width of the cylinder
f	friction factor, $[\Delta p_x/(0.5\rho u_{av}^2)](L_c/L_x)$
h	local heat transfer coefficient
H	height of the channel (non-dimensional)
G_x	streamwise spacing between the cylinders (non-dimensional)
G_y	transverse spacing between the cylinders (non-dimensional)
K	thermal conductivity of fluid/solid
L_c	minimum of A and B
L_x	streamwise extent of the periodic domain (non-dimensional)
L_y	transverse extent of the periodic domain (non-dimensional)
Nu_{xy}	local Nusselt number, $hL_c/K_f = 1/(\theta_w(x,y) - \theta_b(x))$
Nu	average Nusselt number
p	periodic component of pressure (non-dimensional)
Δp_x	axial pressure drop
Pr	Prandtl number, ν/α
Re	Reynolds number, $u_{av}L_c/\nu$
q''	heat flux on the top wall
S	Strouhal number (non-dimensional frequency), sL_c/u_{av}
s	frequency of vortex shedding
t	time (non-dimensional)
T	total temperature
u, v, w	non-dimensional velocities in x, y, and z directions
x, y, z	non-dimensional Cartesian coordinates

Greek symbols

α	thermal diffusivity
$\beta(t)$	mean pressure gradient
ε_{ijk}	alternating tensor
δ_{ij}	Kronecker delta
γ	mean temperature gradient, $1/(HRePr)$
η	thermal performance factor, $\eta = (Nu/Nu_{ch})/(f/f_{ch})^{1/3}$
θ	non-dimensional periodic component of temperature, $q''L_c/K_f$
ρ	density of the fluid/solid
ν	kinematic viscosity of the fluid
ω_i	instantaneous vorticity, $\varepsilon_{ijk}\partial u_k/\partial x_j$

Subscripts

b	bulk
w	wall
ch	channel without obstacle

produced by vortex shedding and unsteady secondary flow motions induced by the cylinder.

A perusal of the relevant literature reveals a fairly large body of literature dealing with flows in channels with vortex generators. Amon et al. [6] have performed a combined numerical and experimental study of self-sustained oscillatory flows in communicating channels. The geometric parameters were selected in order to excite and sustain the Tollmien–Schlichting modes. Wang and Vanka [7] reported a computational study of fluid flow and heat transfer in a periodic array of wavy passages with constant wall temperatures of the confining walls. Their investigation shows that the flow is unsteady after a critical Reynolds number of around 180. The heat transfer is found to be about 2.5 times the smooth channel in the transitional flow regime. The corresponding friction factor was found to be twice that of plane channel flow. In a recent study, flow and heat transfer calculations have been reported in a periodic array of plate-fins by Zhang et al. [8]. Comparisons between steady and unsteady calculations were performed, and it was observed that both the friction and Colburn factors were overpredicted by the two-dimensional simulations. Zhang et al. [9] have also compared the performance between in-line and staggered plate-fin arrangements. They found that staggered arrangements result in higher friction and Colburn factors. Valencia [10] has numerically investigated the flow and heat transfer in a channel with periodically mounted cylinders with axis parallel to the channel walls. His study shows that unsteady oscillatory flows lead to higher heat transfer rates due to the higher mixing of the core fluid and the hot fluid near the walls. In a recent two-dimensional numerical study by Balachandar and Parker [11], the effect of streamwise and transverse pitch of the periodic array of rectangular cylinders on the critical Reynolds number (where unsteadiness is initiated) has been explored. Both inline and staggered arrangements were considered and a one-dimensional linear stability analysis was used to discuss the different flow behavior. With streamwise or transverse periodicity, an early transition to flow unsteadiness was observed (relative to the isolated cylinder). The transverse periodicity appears to have the most important role in determining the critical Reynolds number.

In the present paper, the configuration of interest is a channel with rectangular cross-section cylindrical vortex generators. The cylindrical vortex generator is expected

to enhance the heat transfer in two different ways. One is through the heat conduction from the cylinder that acts as a fin. The second mode of enhancement is through enhanced convection from the heated surface. The enhanced convection is due to large scale unsteadiness, higher turbulence levels, and generation of secondary vortices in the flow. The generation of large scale unsteadiness and secondary vortices requires that the flow rate be above a critical value at which the flow becomes three-dimensional and unsteady. This critical Reynolds number depends on different parameters such as cylinder dimensions and periodic pitch lengths. In the present paper, a pin-fin heat exchanger, with an in-line array of square or rectangular fins are considered and the role of the various geometrical parameters are explored.

The geometry considered is representative of the narrow trailing edge region of a turbine blade where pin fins are used for both structural integrity and heat transfer [12–14]. The present configuration also corresponds to a new strategy for enhanced cooling proposed by Marques [15] in which the blade surface is overplated with cylindrical micro-structures. Coolant is then injected through the micro-structured coolant passage. This arrangement is shown to have high cooling effectiveness [15].

In the present study, only one geometrically-periodic module is considered for an in-line array of cylinders. The decision to impose flow periodicity across one geometrically-periodic module is based on computational economy. Using two or more periodic modules in both streamwise and transverse directions requires additional grid points (to maintain the same resolution), and is computationally expensive. In the past, different researches [9,10] have used one periodic module and successfully simulated the flow and heat transfer in a fin-array geometry.

The baseline geometrical dimensions considered correspond to the micro-structured coolant passage of Marques [15]. A uniform heat flux is applied on one wall (representing the surface exposed to hot gases or heated component) while the opposite wall is adiabatic. Of specific interest is the level of enhancement induced by the change in the aspect ratio of the cylinders and the height of the channel and the evaluation of the thermal performance of such heat exchangers for potential cooling applications.

2. Solution procedure

The geometrical model of the problem to be studied is presented in Fig. 1. The cylinders of dimensions, $A \times B$, form a periodic pattern with streamwise and transverse pitch of L_x and L_y respectively. Only a single periodic module in both the streamwise and transverse directions is considered in the present study. Computations are carried out for various dimensions of the cylinder (A/B) and channel height (H). The streamwise pitch, L_x and transverse pitch, L_y are also varied. However, the streamwise (G_x) and transverse (G_y) spacing between the cylinders are always equal to each other and kept constant. This implies that for $A/B \neq 1.0$, the streamwise and transverse pitch L_x and L_y are not the same. The properties of the fluid and the solid material

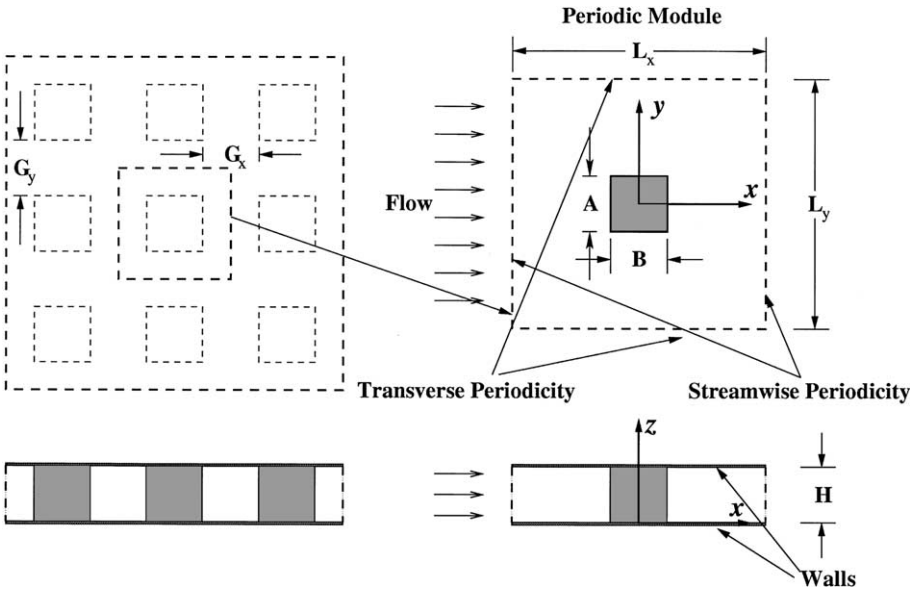

Fig. 1. Computational model of the problem.

chosen in the present study are water and nickel respectively.

Parameters varied in the computation are as follows.

Re (based on minimum cylinder dimensions, L_c): 180–600
A/B: 0.5–2.0
H: 2.5–6.35
L_x: 2.5–7.5
L_y: 2.5–7.5

These represent 19 different cases that are computed and presented in the present study. The imposition of periodic boundary conditions for the dependent variables needs special attention. Patankar et al. [16] have shown that a modified pressure and temperature, obtained by subtracting the mean streamwise variations, satisfy the periodic conditions. A similar approach has also been used by several other researchers [6,8]. The non-dimensional continuity, momentum and energy equations with streamwise and transverse periodic conditions are given by

$$\frac{\partial u_i}{\partial x_i} = 0 \tag{1}$$

$$\frac{\partial u_i}{\partial t} + \frac{\partial}{\partial x_j}(u_j u_i) = -\frac{\partial p}{\partial x_i} + \delta_{i1}\beta(t) + \frac{1}{Re}\frac{\partial^2 u_i}{\partial x_j^2} \tag{2}$$

$$\frac{\partial \theta}{\partial t} + u\gamma + \frac{\partial}{\partial x_j}(u_j \theta) = \frac{1}{Re\,Pr}\frac{\partial^2 \theta}{\partial x_j^2} \tag{3}$$

where $\beta(t)$ is the linear component of the non-dimensional pressure that has to be adjusted in each time step to get the desired mass flow rate. The term, $\beta(t)$, is expressed mathematically as follows:

$$\beta(t) = \beta(t)_{\text{old}}\left[1.0 + \zeta\left\{\left(\frac{u_{\text{av,d}}}{u_{\text{av,p}}}\right)^2 - 1.0\right\}\right] \quad \text{for} \left(\frac{u_{\text{av,d}}}{u_{\text{av,p}}}\right) \leqslant 1.0$$

$$= \beta(t)_{\text{old}} + \left[\zeta\left\{\left(\frac{u_{\text{av,d}}}{u_{\text{av,p}}}\right)^2 - 1.0\right\}\right] \quad \text{for} \left(\frac{u_{\text{av,d}}}{u_{\text{av,p}}}\right) > 1.0$$

where, $u_{\text{av,d}}$ and $u_{\text{av,p}}$ are the desired ($=1.0$) and present iteration average velocities at the inlet periodic plane respectively, and ζ is the relaxation factor whose value is adjusted for optimal convergence in each simulation. Similarly, the linear part of the temperature, γ, is obtained from the global energy balance. In the above equations the velocities are non-dimensionalized with the average velocity u_{av}, all lengths are scaled with the dimensions of the rectangular cylinder, L_c (either A or B), pressure is scaled with ρu_{av}^2 and time is scaled by L_c/u_{av}. The temperature is non-dimensionalized using $q'' L_c/K_f$.

Periodic boundary conditions are used for velocities, pressure and temperature in the streamwise and transverse directions. The channel and cylinder surfaces are treated as no-slip boundaries. Constant heat flux boundary condition is applied on the heated top wall whereas the bottom wall is insulated. A single domain approach is used to solve the conjugate heat transfer problem. The same energy equation is used for both the fluid as well as the solid domain with a higher conductivity (corresponding to nickel alloy) and zero velocity within the solid cylinder. Since a conservative scheme is employed, and the grid distribution is tailored such that mesh boundaries lie along the edges of the cylinder, energy conservation is satisfied automatically across the solid interface.

The differential equations (1)–(3) are solved on a staggered grid by using a modified version of the MAC algorithm of Harlow and Welch [17]. In the present study, convective and diffusion terms are approximated by a second order central differencing scheme. An explicit, second order, Adams–Bashforth differencing scheme is used for the time advancement of the convection and diffusion terms. Once the corrected velocities are obtained using continuity and momentum equations, the energy equation is solved using second order temporal (Adams–Bashforth) differencing scheme. However, the convective and diffusive terms of the energy equation are discretized using third order upwinding scheme of Kawamura et al. [18] and second order central differencing scheme respectively. The detail of the numerical method is described elsewhere [5].

The present simulations are carried out using a minimum grid size of $62 \times 62 \times 42$ for $A/B = 1.0$, $H = 2.5$, $L_x = L_y = 2.5$ while a maximum grid size of $122 \times 122 \times 42$ has been used for $A/B = 1.0$, $H = 2.5$, $L_x = L_y = 7.5$. The computations for the intermediate pitch lengths, aspect ratio and channel height are done with proportionate sized grids. A non-uniform mesh with cells packed toward the solid boundaries has been used to resolve the near-wall viscous effects.

Grid independence was established for $A/B = 1.0$, $L_x = L_y = 5.0$, at a $Re = 400$ by performing computations for two mesh sizes: a $100 \times 100 \times 42$ mesh and $84 \times 84 \times 32$ mesh sizes. The time- and space-averaged Nusselt number and friction factor were found to be 12.45 and 7.08 respectively for a grid size of $84 \times 84 \times 32$ while solution with a mesh size of $100 \times 100 \times 42$ gives a values of 12.12 and 7.39 respectively. The two sets of results show a difference of less than 5% on both mesh sizes and the results are considered to be grid-independent. Therefore, a mesh size of $100 \times 100 \times 42$ was used for this case, and in all other cases considered, comparable mesh dimensions were used, with the number of grid points were scaled up with the geometry.

The present code has been validated thoroughly with the published results for a smooth channel flow. The friction factor and Nusselt have been compared with the analytical values and have been found to be in excellent agreement [5]. The same code has also been tested for the flow past a square cylinder placed in an infinite medium. The Strouhal number and drag coefficient were found to match with the published results 5% [19]. Computations are performed with water as the working fluid whose Prandtl number is 6.99.

3. Results and discussion

Results will be presented in this section to highlight various parametric effects. These include (1) the effect of Reynolds number, (2) the effect of pitch, (3) effect of cylinder aspect ratio, and finally (4) the effect of channel height.

The comparisons among different cases are made using both the instantaneous snapshots of the flow and heat transfer fields, and the averaged (space- and time-averaged in case of unsteady flow) integral parameters, namely friction factor and the Nusselt number. The flow field for the unsteady cases is averaged over a total time of 40–50 time periods corresponding to dominant frequency present in the flow field. The local Nusselt number on the heated top plate is given by

$$Nu = \frac{hL_c}{K_f} = \frac{1}{(\theta_w(x,y) - \theta_b(x))}$$

and friction factor is defined by

$$f = \frac{\Delta p_x}{1/2\rho u_{av}^2}\left(\frac{L_c}{L_x}\right)$$

where Δp_x is the axial pressure drop. The Nusselt numbers reported in the present paper correspond only to the upper heated wall. The cylinder surfaces are not included, as the wall temperature almost equals the bulk temperature at certain locations on the cylinder surface and this results in higher uncertainty in the value of Nusselt number on the cylinder surface.

In order to assess the heat transfer versus pressure drop performance, it is also useful to define a parameter called thermal performance factor (TPF) as

$$\eta = \frac{Nu/Nu_{ch}}{(f/f_{ch})^{1/3}}$$

3.1. Effect of Reynolds number

The long-time integration of the Navier–Stokes equations from the initial flow field ($u = 1.0$, $v = w = 0$, $p = 1.0$ and $\theta = 0.5$) for each configuration of the system reveals that there is a critical Reynolds number above which the flow becomes unsteady. The different cases with their numerically computed state of flow (steady or unsteady) have been tabulated in Table 1. For flow around a square cylinder in an infinite medium, the critical Reynolds number is in the range 50–55 and the associated flow is predominantly two-dimensional [20].

Table 1
Summary of the integral parameters

Simulation	*Re*	State of flow	f/f_{ch}	Nu/Nu_{ch}	η
$A/B = 1.0$,	180	Steady	6.75	2.32	1.24
$H = 2.5$,	250	Steady	6.82	2.88	1.52
$L_x = 2.5$,	400	Unsteady	7.61	4.51	2.29
$L_y = 2.5$	600	Unsteady	22.39	17.13	6.08
$A/B = 0.5$,	180	Steady	6.93	1.57	0.82
$H = 2.5$,	250	Unsteady	9.21	4.67	2.23
$L_x = 3.5$,	400	Unsteady	11.95	8.29	3.63
$L_y = 2.5$	600	Unsteady	16.40	13.20	5.20
$A/B = 2.0$,	180	Steady	9.54	2.32	1.09
$H = 2.5$,	250	Steady	9.67	2.78	1.30
$L_x = 2.5$,	400	Unsteady	23.46	13.58	4.74
$L_y = 3.5$	600	Unsteady	35.08	23.36	7.14
$A/B = 1.0$,	180	Steady	1.93	1.32	1.06
$H = 2.5$,	250	Unsteady	4.97	8.21	4.81
$L_x = 5.0$,	400	Unsteady	7.39	12.12	6.22
$L_y = 5.0$	600	Unsteady	10.14	14.95	6.91
$A/B = 1.0$, $H = 2.5$, $L_x = 7.5$, $L_y = 7.5$	400	Unsteady	4.04	10.30	6.47
$A/B = 1.0$, $H = 4.25$, $L_x = 2.5$, $L_y = 2.5$	400	Unsteady	3.97	8.43	5.21
$A/B = 1.0$, $H = 6.35$, $L_x = 2.5$, $L_y = 2.5$	400	Unsteady	1.54	6.54	5.66

The present flow configuration shows three-dimensional behavior at all Reynolds number even when the flow is steady. The critical Reynolds number in most of the cases is in the range of 180–400, and is therefore at least four times greater than the cylinder placed in an infinite medium. The differences in the transition behavior with that of flow past a cylinder placed in an infinite medium are not unexpected since the present geometry has confining walls in one direction and periodic boundaries in the other two directions.

To illustrate some of the essential flow features, results are first presented for $L_x = L_y = 5.0$, $A/B = 1.0$ and $H = 2.5$. Fig. 2 presents contours of the spanwise component of vorticity, ω_z, for $Re = 180$ and 400 at the mid-span of the cylinder. The flow is naturally steady at Reynolds number of 180 (Fig. 2(a)) and it can be seen that the flow upstream of the cylinder (in the central recirculation region) is stronger than downstream of the cylinder. The flow separates at the leading edges, then reattaches along the side walls of the cylinder and finally separates at the trailing edges. At $Re = 400$, the flow is unsteady as evident from the irregular pattern of the instantaneous vorticity distribution (Fig. 2(b)) that changes with time. The separating shear layers at the leading edges show structures that are smaller and not as well-ordered as that observed for a square cylinder placed in an infinite medium, which exhibits a classical Kármán vortex street where the structures scale with the cylinder diameter, and shed alternately in a regular manner. In the present configuration, the periodicity in the two spatial directions forces interactions between vortical structures shed from the adjacent cylinders, and this generates the less orderly smaller eddies seen in Fig. 2(b).

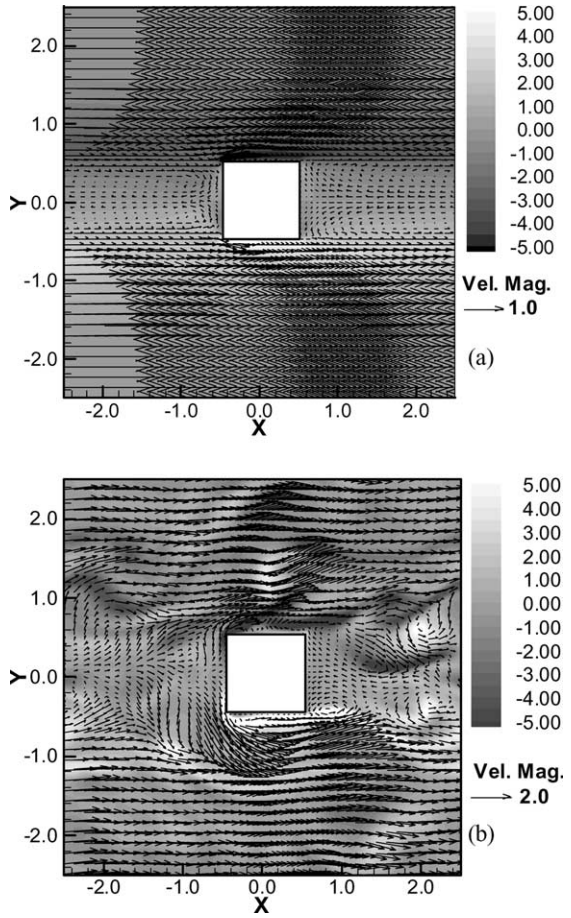

Fig. 2. Distribution of velocity vectors instantaneous superimposed on spanwise vorticity contours at mid-span ($z = 1.25$) for (a) $Re = 180$ (steady flow) and (b) $Re = 400$ for $L_x = L_y = 5.0$, $A/B = 1.0$ and $H = 2.5$. The maximum and minimum values of the non-dimensional vorticity in the computational domain are about ± 31.0 but in Fig. 2(b) results are plotted for a vorticity range of ± 5.0 for clarity.

Fig. 3 shows the temperature field of the upper heated wall corresponding to the Reynolds number of 180

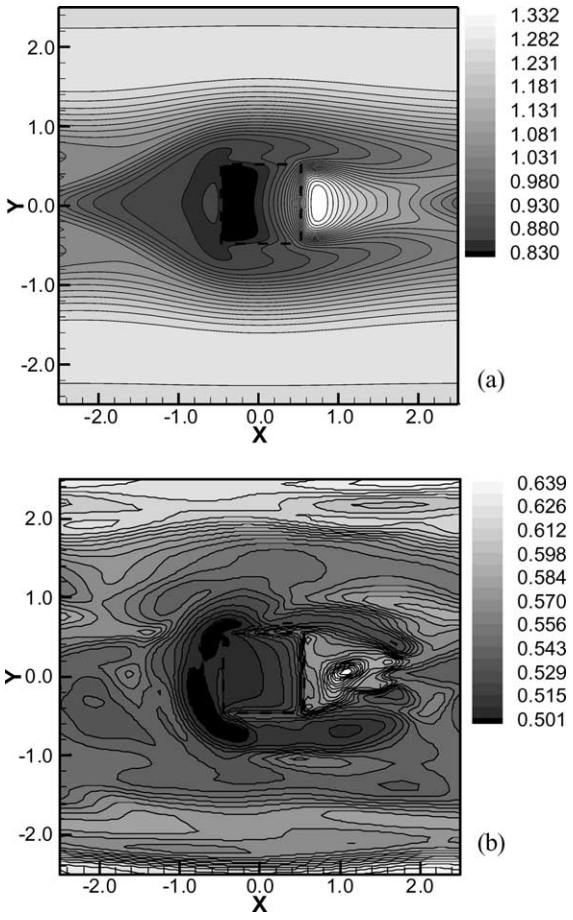

Fig. 3. Instantaneous top wall temperature at (a) $Re = 180$ (steady flow) and (b) $Re = 400$ for $L_x = L_y = 5.0$, $A/B = 1.0$ and $H = 2.5$.

and 400. It is evident that the wall temperatures upstream of the cylinder are lower than the temperatures in the region downstream of the cylinder. The three-dimensionality of the flow and transverse mixing are the strongest in the region upstream of the cylinder and this contributes to correspondingly higher heat removal rates and lower temperatures. Though the secondary flow is weak for the steady flow at $Re = 180$, they become important near the channel–obstacle juncture, and cylinder surfaces. The lowest temperatures are obtained in the cylinder region itself and immediately or the upstream of the cylinder. The cylinder acts as a heat sink drawing heat from the wall and dissipating it to the fluid across the various faces of the cylinder. At $Re = 400$, the unsteady nature of the flow can lead to convective heat transfer rates greater than conduction heat transfer rates, as evidenced by the lowest temperatures located upstream of the cylinder. Due to the unsteady flow motion and the generation of the secondary vortices, pockets of cold fluid from the lower part of the channel are transferred upwards to cool the wall. As a consequence, cold spots are seen on the top heated wall and this leads to wall temperature distributions that are irregular in space. Comparison of Fig. 3(a) and (b) reveals that the wall temperature is about two times higher for the steady flow at $Re = 180$ than for the unsteady flow at $Re = 400$.

Fig. 4 shows the corresponding temperature contours along the cross-stream plane $x/B = 0$. The thermal field at $Re = 180$ (Fig. 4(a)) is seen to be symmetric about the centerline with a clear temperature variation along the vertical and transverse directions representing the fin-heat-sink effect. For $Re = 400$ (Fig. 4(b)), the thermal boundary layer on the top surface is seen to be considerably thinner and quite convoluted due to the unsteady nature of the strong secondary vortices which disrupt the thermal boundary layer and results in higher heat transfer rates.

Fig. 5 represents the iso-surfaces of the spanwise component of vorticity ($\omega_z \pm 2.5$) for a Reynolds number of 400. The separating shear layers are almost two-dimensional at the leading corners of the cylinder. The shear layers separate at the leading corner (marked A) and reattaches (in the vicinity of B) and remain attached till they finally separates at the trailing corners (marked C) of the cylinder. An immediate roll-up formation past the trailing edge is not observed, as seen in wakes past bluff bodies placed in an infinite medium. Therefore, immediately downstream of the cylinder, there is less cross-stream entrainment of fluid into the wake region between two consecutive cylinders. However, the shear layers breakdown further downstream becoming complex three-dimensional structures including enhanced entrainment and mixing in front of the preceding cylinder. Fig. 6 represents the iso-surface of streamwise velocity ($u = 1.0$). The lower velocity near the wall and the higher velocity core fluid between in the transverse gap between the two cylinders is obvious from the three-dimensional distribution of the velocity. The gaps ahead and downstream of the cylinder are dominated by recirculatory low velocity flow. The convoluted nature of the iso-surface near the two walls signifies the three-dimensional nature of the boundary layer. The boundary layer in a two-dimensional flow is always two-dimensional. Therefore, the secondary flow in the present three-dimensional flow causes the boundary layer to

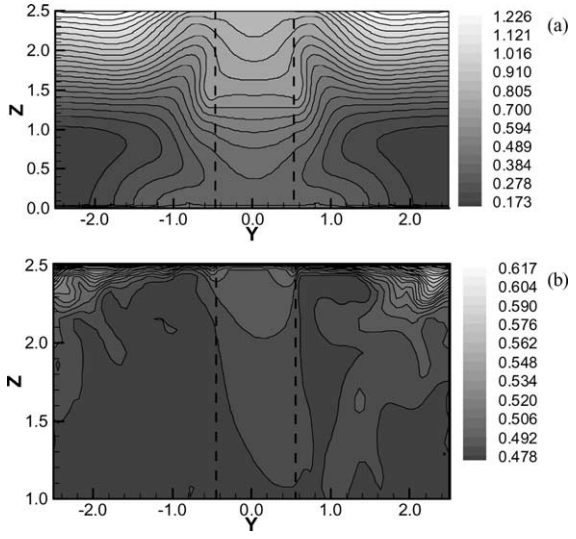

Fig. 4. Instantaneous temperature distribution at the mid-streamwise location ($x = 0.0$) for (a) $Re = 180$ and (b) $Re = 400$ for $L_x = L_y = 5.0$, $A/B = 1.0$ and $H = 2.5$.

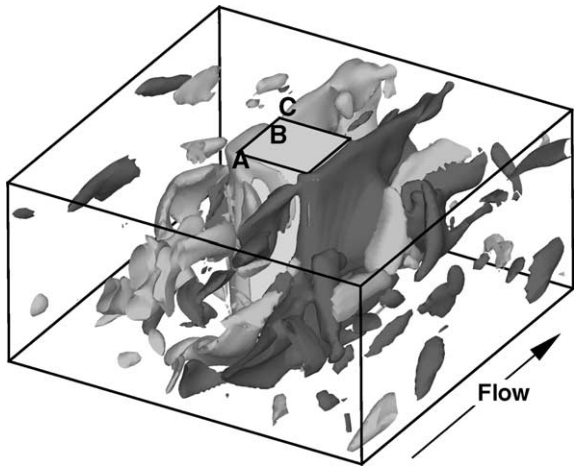

Fig. 5. Iso-surfaces of instantaneous spanwise vorticity ($\omega_z = \pm 2.5$) for $Re = 400$ and $L_x = L_y = 5.0$, $A/B = 1.0$ and $H = 2.5$. Black surface is positive vorticity.

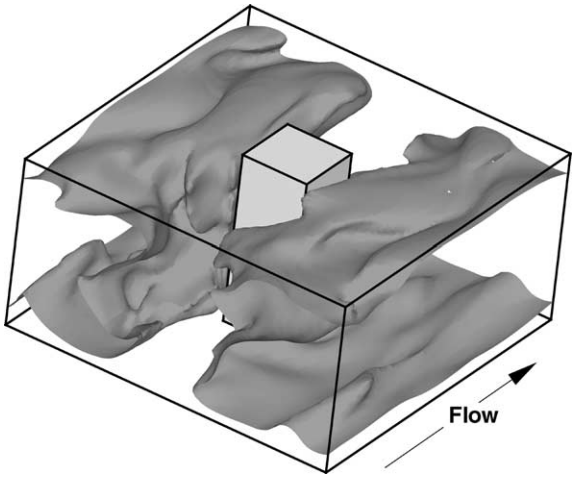

Fig. 6. Iso-surfaces of instantaneous streamwise velocity ($u = 1.0$) for $Re = 400$ and $L_x = L_y = 5.0$, $A/B = 1.0$ and $H = 2.5$.

become three-dimensional. The three-dimensional spatial distribution of a selected isotherm ($\theta = 0.49$) is shown in Fig. 7 where, for clarity, the geometry has been inverted around the horizontal axis, so that the lower surface represents the heated surface. Near the periodic boundaries and downstream of the cylinder, where the flow velocity and thermal gradients are low, the isotherm is lifted off the surface to a relatively greater spanwise extent. In regions where the thermal gradients are high (in the cylinder region and upstream of the cylinder) the isotherm ($\theta = 0.49$) is expectedly closer to the heated surface. Another interesting observation in the isotherm is revealed in the region near the junction of channel wall and the cylinder. The isotherm is seen to be pressed to-

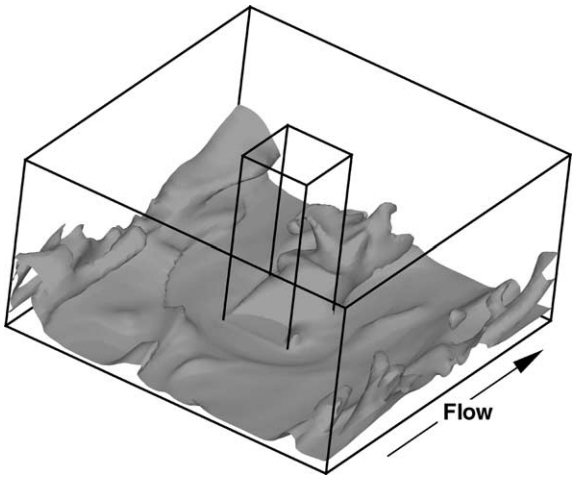

Fig. 7. Iso-surfaces of instantaneous temperature ($\theta = 0.49$) for $Re = 400$ and $L_x = L_y = 5.0$, $A/B = 1.0$ and $H = 2.5$.

wards the channel wall indicating the higher interaction of the wall boundary layers from the channel walls and cylinder wall and the secondary vortices. There appears to be some correlation between the iso-surface of streamwise velocity in Fig. 6 and isotherms in Fig. 7. The streamwise velocity influences the temperature field most. The region of higher velocity reveals low temperature and vice versa.

Table 1 shows the variation of friction factor and Nusselt number for four different configurations at different Reynolds numbers. For each configuration, both the friction factor as well as the Nusselt number increases significantly when the flow switches from a steady to an unsteady state. Note that at $Re = 600$ (unsteady flow), Nu/Nu_{ch} reaches values in the range of 10–20 for certain geometrical parameters. At $Re = 600$, the aspect ratio $A/B = 2.0$ appears to provide the highest heat transfer enhancements (23.36) and higher TPFs ($\eta = 7.14$). These high levels are quite promising compared to typical enhancement levels of the order of 2–3 for rib turbulators [21] and 3–4 for pin-fin turbulators [14] for a Reynolds number of the order of 5×10^3–10^4. The lower ranges for the pin-fin turbulators reported in the literature appear to stem from the choice of geometrical parameters (based either on poor design or geometrical constraints imposed by other requirements) and the higher fully turbulent Reynolds number regime of interest. In the present study, $Re \leqslant 600$, and the flow is steady and laminar for the baseline channel flow cases. In the presence of cylinders, the flow becomes unsteady having multiple frequencies. Increase in Reynolds number adds to the number of frequencies, but the flow does not become fully turbulent even at the maximum Reynolds number considered in the present work. The unsteadiness in the flow induced by the cylinder results in very high heat transfer rates compared to the steady, laminar plain channel flow. Thus the heat transfer can be enhanced significantly choosing geometrical and operational parameters in such a way that large scale self-sustained unsteady structures are generated in the flow field. The large scale vortices have more energy and therefore are very effective in transferring thermal energy from channel wall into the core of the fluid. On the other hand, with small scale turbulence near the wall, the benefits of the large scale unsteadiness are not realized, and more modest heat transfer enhancements, as reported in the literature, can only be realized.

Fig. 8 depicts the variation of TPF with Reynolds number for different sets of geometrical parameters. In general, η for steady flows varies between 1 and 2, where for unsteady flows it varies between 2 and 7. The higher pitch case $L_x = L_y = 5.0$ ($A/B = 1$) generally shows the highest TPF over most of the Reynolds number range. In the range of parameters studied, it would appear that the higher pitch ($L_x = L_y = 5.0$) and the higher aspect ratio (A/B) may provide the best results. In one case

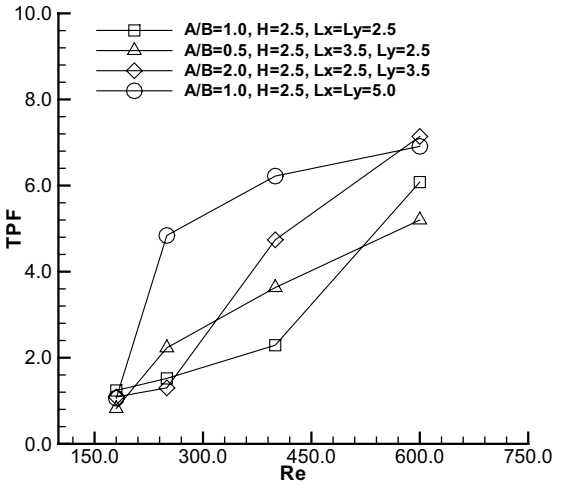

Fig. 8. Dependency of TPF with various Reynolds number at different geometric configuration.

($A/B = 0.5$, $H = 2.5$, $L_x = 3.5$, $L_y = 2.5$), η goes below unity, which is not desirable for a good heat exchanger. In this case, the flow is steady in nature.

3.2. Effect of pitch

In the present paper, simulations were done using three different pitch lengths. The present section discusses the cases having pitch a $L_x = L_y$ of 2.5, 5.0 and 7.5 while the other parameters such as H and A/B are kept constant. Since the computation having a pitch of 7.5 requires higher computational resources, only a single simulation has been carried out at $Re = 400$. For configurations with the lower pitch of $L_x = L_y = 2.5$, ($H = 2.5$, $A/B = 1.0$), the flow is found to be steady at Reynolds number of 180 and 250. Similarly, with the configuration, $L_x = 2.5$, $L_y = 3.5$, $H = 2.5$, $A/B = 2.0$, the flow at $Re = 180$ and 250 results in a steady state condition. The flow at this lower pitch is similar to the flow in a communicating channel where the recirculation occupies the entire gap between the cylinders [8]. As the pitch is increased, say to 5.0, the flow becomes unsteady at a lower Reynolds number of 250. To illustrate the influence of the pitch on the flow field, Fig. 9 shows the mid-span spanwise vorticity (ω_z) contours superimposed on the velocity vector plot for $Re = 400$ and a pitch of 2.5 and 7.5 respectively. The corresponding plot for a pitch of 5.0 was shown earlier in Fig. 2(b). At a pitch of 2.5, two counter rotating vortices are formed in the gap. These vortices remain trapped in the inter-cylinder region and do not shed downstream. There is no flow separation at the leading corners of the cylinders and thus flow remains attached on the side walls of the cylinder. The flow between the cylinder and the transverse periodic planes is similar to fully developed flow in a

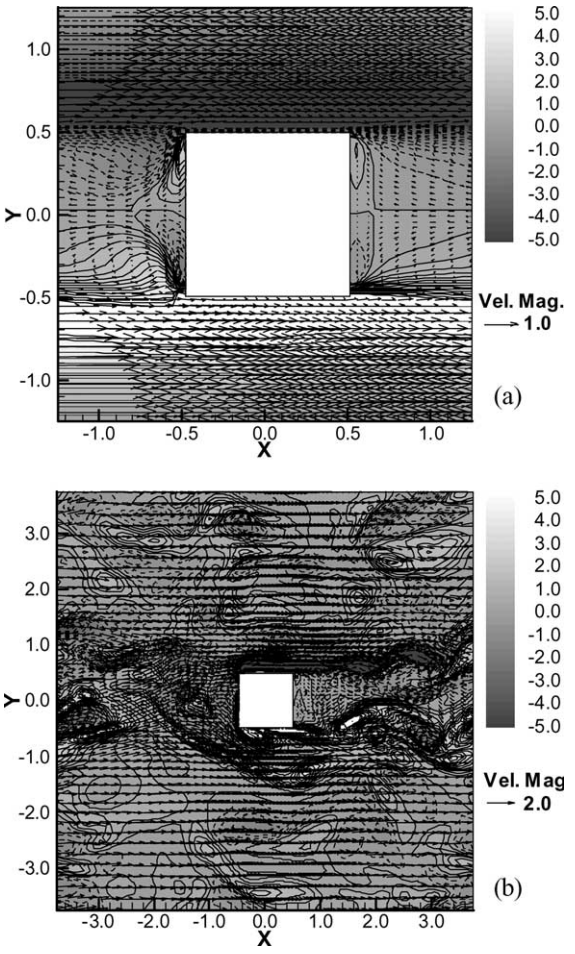

Fig. 9. Distribution of instantaneous velocity vectors superimposed on spanwise vorticity contours at mid-span ($z = 1.25$) for (a) $L_x = L_y = 2.5$ and (b) $L_x = L_y = 7.5$ for $Re = 400$, $A/B = 1.0$ and $H = 2.5$.

channel. The flow field having a pitch of 5.0 (Fig. 2(b)) and a pitch of 7.5 (Fig. 9(b)) reveals clear shedding patterns. Clearly as the pitch decreases, unsteadiness and vortex shedding is diminished (compare Fig. 9(a) and (b)) and thus the transition process is delayed by the decrease in the pitch of the periodic cylinders. However, Figs. 2(b) and 9(b) also reveal that as the pitch is increased from 5.0 to 7.5 the flow structures that are shed exhibit less cylinder to cylinder interactions.

The streamwise vorticity, ω_x (representing the strength of the secondary flow) at the mid streamwise plane are shown in Fig. 10 for the two different pitches 2.5 and 7.5. It is clear that the damping due to the closer proximately of the cylinder at the lower pitch makes the secondary flow weaker and the flow in Fig. 10(a) is seen to be only weakly unsteady with two large counter-rotating eddies in the cross-stream plane. The weak unsteadiness at the lower pitch is linked to the fact that the

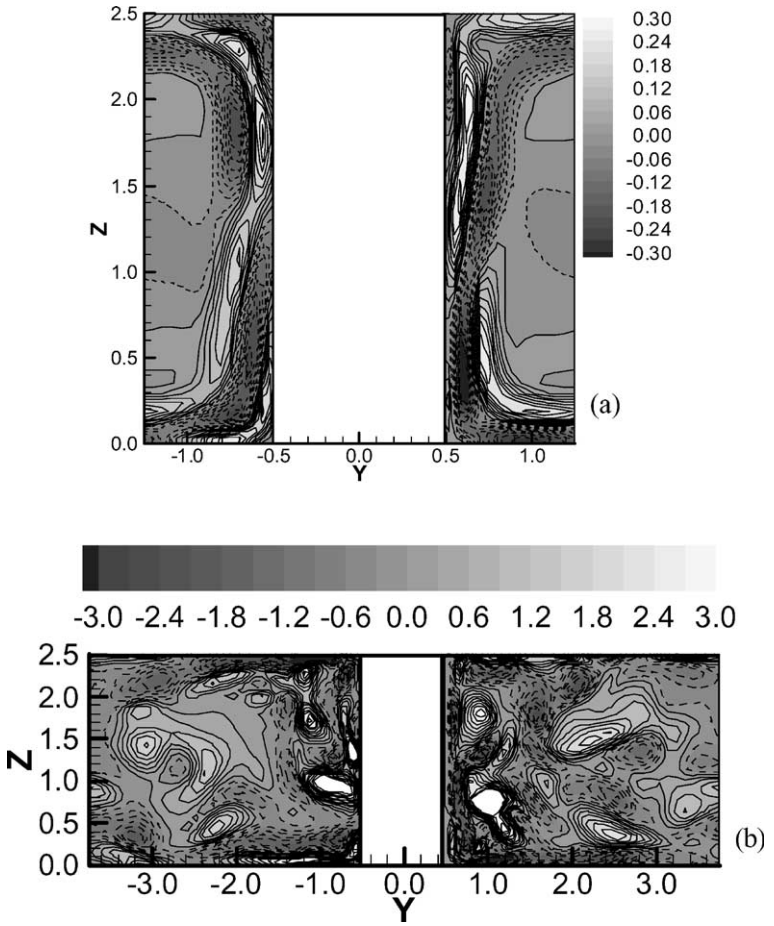

Fig. 10. Distribution of instantaneous streamwise vortices (secondary flow) at the mid-streamwise plane ($x = 0$) for (a) $L_x = L_y = 2.5$ and (b) $L_x = L_y = 7.5$ for $Re = 400$, $A/B = 1.0$ and $H = 2.5$.

flow between the two transverse cylinders behaves like a channel flow and the driving mechanisms for unsteadiness such as flow separation and vortex shedding are weak. For the larger pitch, the flow is strongly unsteady with secondary eddies (positive and negative vorticity) circulating in the cross-stream plane (Fig. 10(b)).

Table 1 shows that at $Re = 400$, as the pitch is increased from 2.5 to 7.5, the TPF increases monotonically by a factor of nearly 3, while the friction factor ratio decreases by a factor of 2. However, the heat transfer enhancement is highest at a pitch of 5.0 ($Nu/Nu_{ch} = 12.12$), and decreases to 10.30 at a pitch of 7.5. The non-monotonic behavior in the heat transfer is linked to the fact that as the pitch is increased from 2.5 to 5.0, vortex shedding and flow unsteadiness increases (see Figs. 2 and 9), but increasing the pitch further to 7.5 leads to a reduction in the interaction between the vortical structures (since cylinder are placed further apart). This from a heat transfer perspective, there appears to be an optimum pitch value.

At the lower pitch of 2.5, due to the high blockage ratios, high velocities are obtained in the transverse region between cylinders, and thus high heat transfer coefficients are found along the transverse edges of the cylinders. Because of this, at sufficiently high Reynolds number, e.g., $Re = 600$, the highest heat transfer enhancement is obtained at a pitch of 2.5. Therefore, the optimal pitch for maximizing the heat transfer appears to be Reynolds number dependent.

3.3. Effect of aspect ratio of cylinder

The aspect ratio is defined by the ratio of the cylinder dimension in the transverse direction to that in the streamwise direction. Three aspect ratios (0.5, 1.0 and 2.0) at four different Reynolds numbers (180, 250, 400 and 600) have been chosen for comparison purposes. Both the channel height and the spacings between the cylinders, G_x and G_y are kept constant at 2.5 and 1.5 respectively. Fig. 11 represents the velocity vectors su-

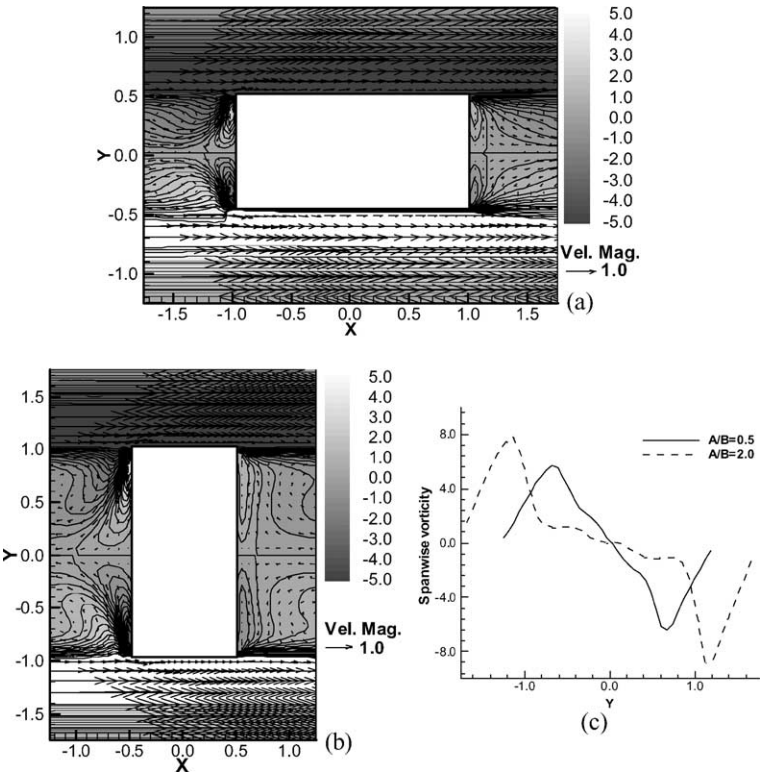

Fig. 11. Distribution of velocity vectors superimposed on spanwise vorticity contours at mid-span ($z = 1.25$) for (a) $A/B = 0.5$, $L_x = 3.5$, $L_y = 2.5$ and (b) $A/B = 2.0$, $L_x = 2.5$, $L_y = 3.5$ for $Re = 180$ and $H = 2.5$, (c) comparison of spanwise vorticity for the two aspect ratio at a location 0.4 upstream of the leading edge of the cylinder.

perimposed on the spanwise vorticity (ω_z) contours at $Re = 180$ for the aspect ratio of 0.5 and 2.0. At this low Reynolds number, as noted earlier, no vortex shedding is observed, and the flow between the cylinders in the transverse direction behaves as in communicating channel at low Reynolds number. For the two different aspect ratios the flow features look similar. Since the spanwise vorticity within the recirculation region is small, the comparison between the two cases is shown through a line plot in Fig. 11(c). The streamwise flow velocity in the transverse region between the cylinders has higher magnitudes for $A/B = 2.0$ due to the higher blockage ratio. As a consequence, lower wall temperature (Fig. 12) and higher heat transfer rates are obtained for this case. In view of the weaker recirculation, a pair of high temperature zones is observed upstream of the cylinder for $A/B = 2.0$ (Fig. 12(b)). The thermal gradient near the cylinder in the transverse direction is very steep at the cylinder interface (or the transverse heat transfer rate) (Figs. 12(b) and 13) and is particularly significant for the higher aspect ratio. This fact is related to the higher blockage in the transverse direction and higher transverse velocity gradient observed in Fig. 11(b). The axial (along the cylinder axis) conduction in case of higher aspect ratio is also more significant (Fig. 12(b)). The strength of the secondary flow in the transverse region between the two cylinders weakens once the aspect ratio is increased from 0.5 to 1.0. However, a further increase in the aspect ratio increases the secondary flow thus giving higher heat transfer rates.

At $Re = 400$, the flow is unsteady and the instantaneous wall temperature contours for the two aspect ratios are shown in Fig. 14. Comparison of Figs. 14(a) and (b) illustrates that the temperature distribution on the wall at aspect ratio of 0.5 is more uniform in the transverse region between the cylinders, but the temperature levels are in general higher (as at $Re = 180$), and particularly so in the recirculation region downstream of the cylinder. The thermal boundary layer development on transverse side walls can be seen for an aspect ratio of 0.5, while it is not as evident for the case of aspect ratio of 2.0. The secondary motion of the flow structures for two aspect ratios are shown in Fig. 15. The strength of the secondary flow is more for aspect ratio of 2.0 (peak values are nearly 30% higher) and the flow structures have smaller length scales. As a result of the stronger secondary flow there is more heat removal

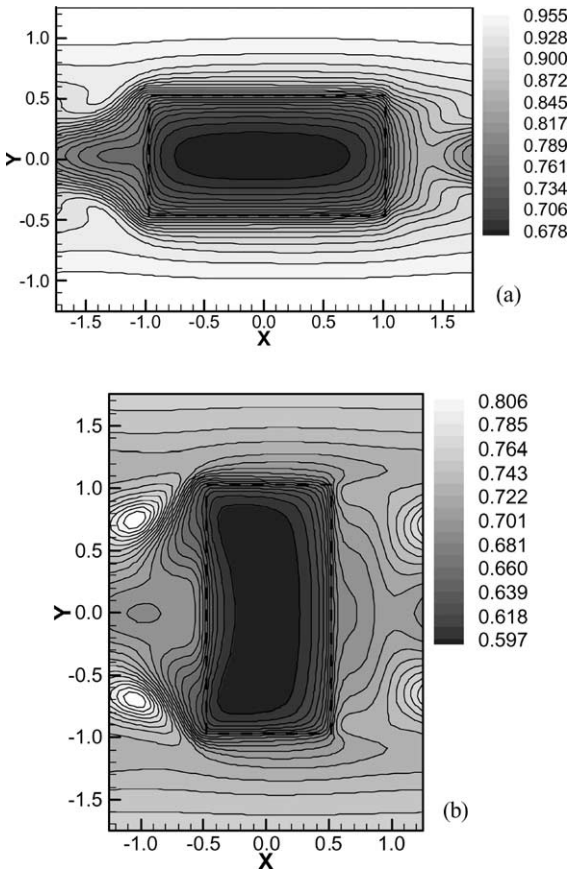

Fig. 12. Wall temperature distribution at (a) $A/B = 0.5$, $L_x = 3.5$, $L_y = 2.5$ and (b) $A/B = 2.0$, $L_x = 2.5$, $L_y = 3.5$ for $Re = 180$ and $H = 2.5$.

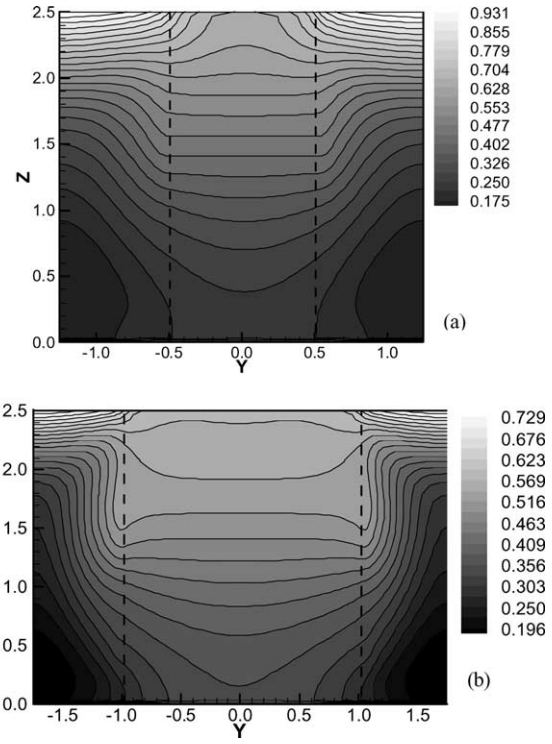

Fig. 13. Temperature distribution at the mid-streamwise plane ($x = 0$) for (a) $A/B = 0.5$, $L_x = 3.5$, $L_y = 2.5$ and (b) $A/B = 2.0$, $L_x = 2.5$, $L_y = 3.5$ for $Re = 180$ and $H = 2.5$.

from the wall and leads to a lower maximum wall temperature.

The variation of TPF at various aspect ratios and for different Reynolds number has been depicted in Fig. 16. The change in aspect ratio results in the change in the form drag. On the other hand, the friction drag depends on the surface quality and the effective length and the state (steady or unsteady) of the flow. The friction factor for aspect ratio of 0.5 is higher than the aspect ratio of 1.0 at $Re = 180$ for which both the flow is steady. There is consistent decrease and increase in the friction factor at all Reynolds numbers with the increase in aspect ratio from 0.5 to 1.0 and 1.0 to 2.0 respectively. However, Nusselt number does not show any such behavior. This particular effect may be due to the flow at $Re = 180$ and aspect ratio of 0.5 where the velocity gradient along the transverse side walls is high and gives higher friction. As discussed earlier, the unsteadiness is weak for aspect ratio of 1.0 and thus gives lower friction factor. In the steady flow regime, the TPF is low (in the range of 1–2) and is relatively insensitive to the aspect ratio. In the unsteady regime, the TPF is the highest at an aspect ratio of 2.0. At $Re = 400$, the TPF variation is non-monotonic reflecting the competition between the enhancement in Nusselt number versus the increase in pressure drop. At $Re = 600$, the unsteady nature of the flow gives significant increase in Nusselt number compared to the frictional pressure drop thus resulting in monotonically increasing TPF values with respect to the aspect ratio.

3.4. Effect of channel height

The effect of channel height is studied by simulating flow for a single Reynolds number of 400 and three channel heights (2.5, 4.25 and 6.35). The other parameters such as pitch and aspect ratio of the cylinder are held constant at 2.5 and 1.0 respectively. Fig. 17 shows the distribution of streamwise vorticity, ω_x, at the mid-streamwise plane ($x = 0$). The secondary flow appears to be the strongest at the intermediate height $H = 4.25$. This is because the damping from the top and bottom walls play an important role at $H = 2.5$, while at $H = 6.35$, the larger cross-sectional area reduces the strength of the secondary flow. The large scale secondary structure for $H = 2.5$ results in higher friction factor

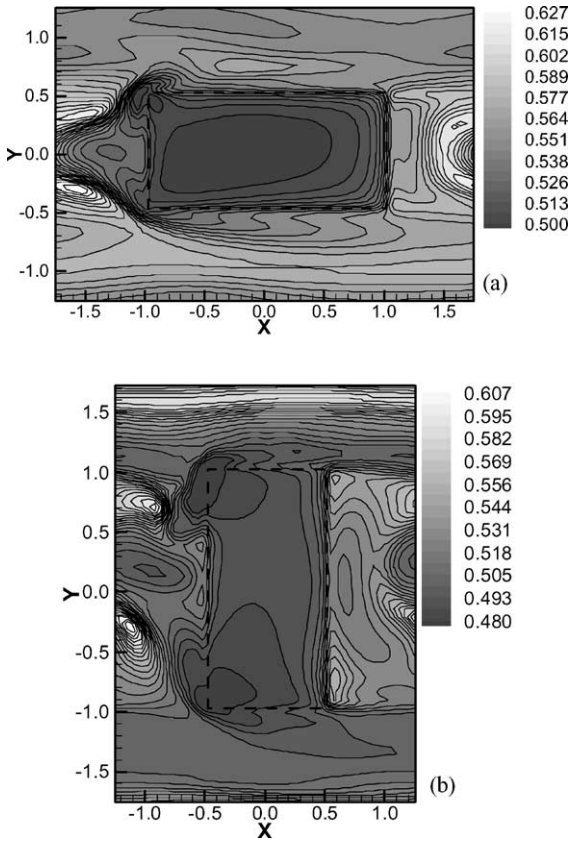

Fig. 14. Instantaneous wall temperature distribution at (a) $A/B = 0.5$, $L_x = 3.5$, $L_y = 2.5$ and (b) $A/B = 2.0$, $L_x = 2.5$, $L_y = 3.5$ for $Re = 400$ and $H = 2.5$.

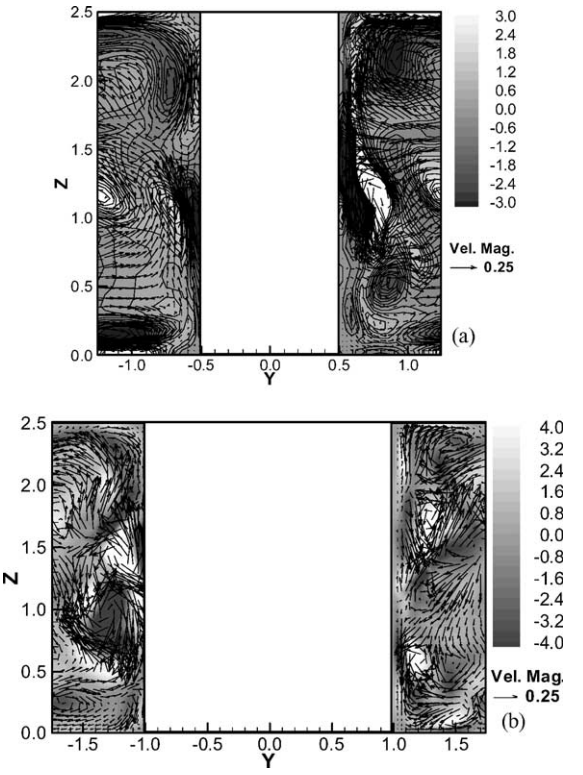

Fig. 15. Distribution of instantaneous velocity vectors superimposed on secondary vorticity (streamwise) contours at mid-streamwise plane ($x = 0$) for (a) $A/B = 0.5$, $L_x = 3.5$, $L_y = 2.5$ and (b) $A/B = 2.0$, $L_x = 2.5$, $L_y = 3.5$ for $Re = 400$ and $H = 2.5$.

(7.61) even though the structure is weaker than the other two channel heights. The temperature distribution at the same location for the three different cases is shown in Fig. 18. Both the penetration of the thermal boundary layer and the temperature gradients at the transverse interfaces are enhanced with $H = 4.25$ and 6.35 where the secondary flows are stronger. Since the Nusselt number enhancement is somewhat related to the strength of the secondary flow, it is highest in case of the intermediate channel height (Table 1). Though the Nusselt number is higher at $H = 4.25$, TPF is the highest (5.66) for $H = 6.35$ because of the lower-pressure drop for this case while it is the highest for $H = 2.5$.

4. Conclusions

A three-dimensional numerical study for fluid flow and heat transfer has been conducted for a parallel plate-channel heat exchanger with periodic in-line array of cylinders. The study was aimed at the effects of Reynolds number and the geometrical parameters on the

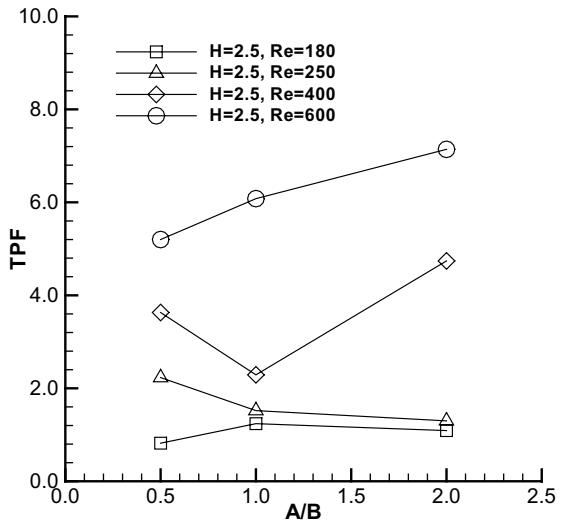

Fig. 16. Dependency of TPF with various aspect ratio of the cylinder at different Reynolds number and geometric configuration.

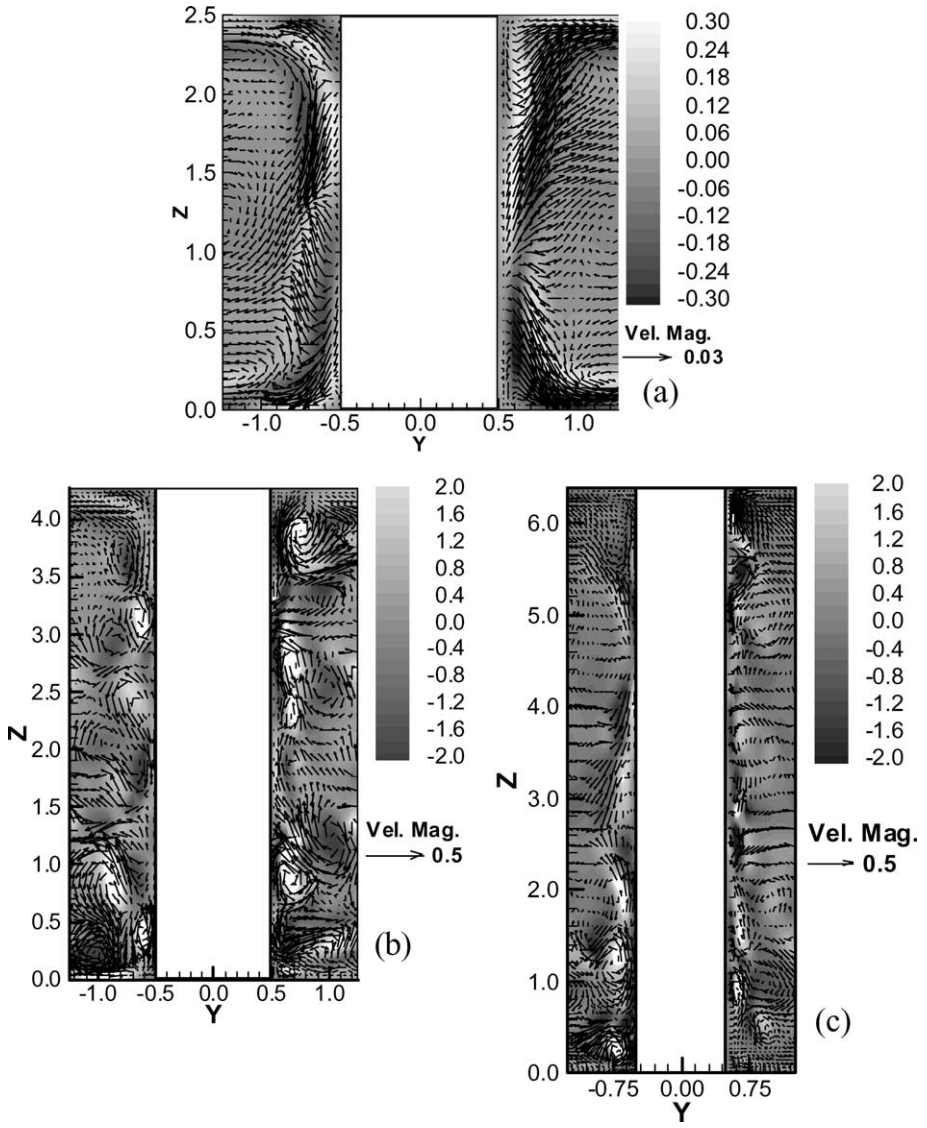

Fig. 17. Distribution of instantaneous streamwise vortices (secondary flow) at mid-streamwise plane ($x = 0$) for (a) $H = 2.5$, (b) $H = 4.25$ and (c) $H = 6.35$ and $L_x = L_y = 2.5$, $Re = 400$ and $A/B = 1.0$.

heat transfer and the friction factor. The following are the conclusions from this study.

1. The flow in each configuration shows three-dimensional behavior at all Reynolds numbers. The flow becomes unsteady in most of the cases above $Re = 180$.
2. The TPF increases significantly when the flow switches from steady to an unsteady state irrespective of the geometrical configurations. The TPF is found to increase with the increase in Reynolds number for each configuration.
3. The aspect ratio (A/B) of the cylinders (pins) is important in the critical or transition Reynolds number where the relative increase in friction factor is more compared to the increase in the heat transfer.
4. The heat transfer is seen to increase with the increase in a pitch from 2.5 to 5.0 but decreases with further increase in pitch. However, the TPF shows an increasing trend with the pitch because of its lower friction factor at higher pitch.
5. The increase in channel height shows a monotonic decrease in friction factor. However, the strength

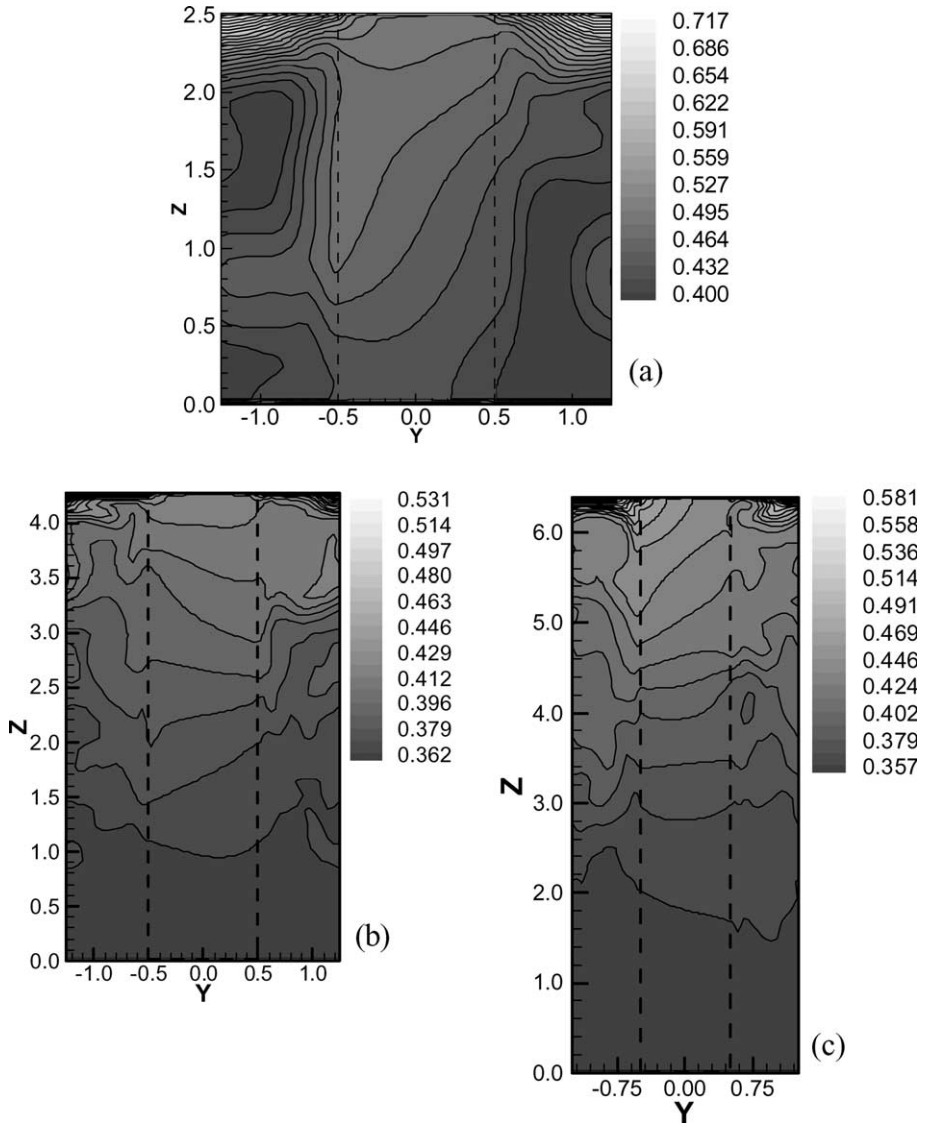

Fig. 18. Distribution of temperature at mid-streamwise plane ($x = 0$) for (a) $H = 2.5$, (b) $H = 4.25$ and (c) $H = 6.35$ and $L_x = L_y = 2.5$, $Re = 400$ and $A/B = 1.0$.

of the secondary flow and the heat transfer increases initially as H is increased from 2.5 to 4.25 but decreases with further increases in channel height.

6. At the highest Reynolds number studied ($Re = 600$) the TPF shows a monotonic increase with the aspect ratio.

Acknowledgements

This work was supported by a grant from DARPA. Their support is greatly acknowledged. We also acknowledge the useful technical discussions with Professor Kevin Kelly and Christopher Marques.

References

[1] R. Mittal, S. Balachandar, Effect of three-dimensionality on the lift and drag of nominally two-dimensional cylinders, Phys. Fluids 7 (1995) 1841–1865.

[2] Y. Chen, M. Fiebig, N.K. Mitra, Conjugate heat transfer of a finned oval tube. Part B. Heat transfer behaviours, Numer. Heat Transfer Part-A 33 (4) (1998) 387–401.

[3] M. Fiebig, Vortex generators for compact heat exchangers, J. Enhanced Heat Transfer 2 (1995) 43–61.

[4] A. Grossegorgemann, D. Weber, M. Fiebig, Experimental and numerical investigation of self-sustained oscillations in channels with periodic structures, Exp. Thermal Fluid Sci. 11 (3) (1995) 226–233.

[5] A.K. Saha, S. Acharya, Three-dimensional flow and heat transfer calculations in micro-channel heat exchangers, HTD-vol. 366-3, Proceeding of the ASME Heat Transfer Division, IMECE 2001, New York, NY, 11–16 November 2001, vol. 3.

[6] C.H. Amon, D. Majumdar, C.V. Herman, F. Mayinger, B.B. Mikic, D.P. Sekulic, Numerical and experimental studies of self-sustained oscillatory flows in communicating channels, Int. J. Heat Mass Transfer 35 (11) (1992) 3115–3129.

[7] G. Wang, S.P. Vanka, Convective heat transfer in periodic wavy passages, Int. J. Heat Mass Transfer 38 (17) (1995) 3219–3230.

[8] L.W. Zhang, D.K. Tafti, F.M. Najjar, S. Balachandar, Computations of flow and heat transfer in parallel-plate fin heat exchangers on the CM-5: effects of flow unsteadiness and three-dimensionality, Int. J. Heat Mass Transfer 40 (6) (1997) 1325–1341.

[9] L.W. Zhang, S. Balachandar, D.K. Tafti, F.M. Najjar, Heat transfer enhancement mechanisms in Inlinein-line and staggered parallel-plate fin heat exchanger, Int. J. Heat Mass Transfer 40 (10) (1997) 2307–2325.

[10] A. Valencia, Heat transfer enhancement due to self-sustained oscillating transverse vortices in channels with periodically mounted rectangular bars, Int. J. Heat Mass Transfer 42 (1999) 2053–2062.

[11] S. Balachandar, S.J. Parker, Onset of vortex shedding in an inline and staggered array of rectangular cylinders, Phys. Fluid 14 (10) (2002) 3714–3732.

[12] B.A. Brigham, G.J. VanFossen, Length-to-diameter ratio and row number effects in short pin fin heat transfer, J. Eng. Gas Turbines Power 106 (1984) 241–246.

[13] D.E. Metzger, S.W.Haley, Heat transfer experiments and flow visualization of arrays of short pin fins, ASME Paper No. 82-GT-138, 1982.

[14] M.K. Chyu, Y.C. Hsing, V. Natarajan, Convective heat transfer of cubic fin arrays in a narrow channel, J. Turbomachinery 120 (1998) 362–367.

[15] C. Marques, Heat transfer in a micro-fabricated channel with an array of cylindrical posts, Ph.D. dissertation, Louisiana State University, Mechanical Engineering Department, 2003.

[16] S.V. Patankar, C.H. Liu, E.M. Sparrow, Fully developed flow and heat transfer in ducts having streamwise-periodic variations of cross-sectional area, J. Heat Transfer 99 (1977) 180–186.

[17] F.H. Harlow, J.E. Welch, Numerical calculation of time-dependent viscous incompressible flow of fluid with free surfaces, Phys. Fluids 8 (1965) 2182–2188.

[18] T. Kawamura, H. Takami, K. Kuwahara, Computation of high Reynolds number flow around a circular cylinder with surface roughness, Fluid Dyn. Res. 1 (1986) 145–162.

[19] A.K. Saha, K. Muralidhar, G. Biswas, Transition and chaos in two-dimensional flow past a square cylinder, ASCE J. Eng. Mech. 126 (5) (2000) 523–532.

[20] A. Sohankar, C. Norberg, L. Davidson, L. Numerical, simulation of unsteady flow around a rectangular two-dimensional cylinder at incidence, J. Wind Engrg. Ind. Aero. 69 (1997) 189–201.

[21] J.H. Wagner, B.V. Johnson, R.A. Graziani, F.C. Yeh, Heat transfer in rotating serpentine passages with trips normal to the flow, J. Turbomachinery 114 (1992) 847–857.